

DEFECT TRANSFORMATION IN INTENTIONALLY CONTAMINATED FZ SILICON DURING LOW TEMPERATURE ANNEALING

H. Habenicht¹, P. Gundel¹, T. Mchedlidze², M. Kittler², G. Coletti³, W. Warta¹

¹Fraunhofer Institute for Solar Energy Systems (ISE), Heidenhofstr. 2, 79110 Freiburg, Germany

²IHP/BTU Joint Lab, E.-Weinert-Str. 1, 03046 Cottbus, Germany

³Energy research Centre of the Netherlands (ECN) Westerduinweg 3, NL-1755 LE Petten, The Netherlands

Corresponding author: Holger Habenicht, +49(0)761/4588-5461, Holger.Habenicht@ise.fraunhofer.de

Silicon samples intentionally contaminated with iron during growth were investigated in the as-grown state and after a prolonged low temperature anneal at around 300°C with different characterisation techniques, i.e. Deep Level Transient Spectroscopy (DLTS), Temperature Dependent Lifetime Spectroscopy (TLDS) and Photoluminescence (PL) spectroscopy. A defect transformation was found, changing the type of defect from iron-related complexes to interstitial iron.

Keywords: Multicrystalline Silicon, Spectroscopy, Defects

1 INTRODUCTION

For the improvement of solar cells made from multicrystalline (mc) silicon the principal understanding of the influence of impurities is essential. This holds true especially if lower quality silicon feedstock shall be used leading to a higher impurity level.

The goal of this work was to obtain an improved understanding of the types of defects acting as recombination centres in mc silicon wafers. A large variety of impurities, present in low quality feedstock and their interaction with each other and with structural defects, i.e. grain boundaries and dislocations, seriously complicates investigations of their influence on the material. To overcome this difficulty we used samples intentionally doped with only one kind of impurity, in the present case with iron as impurity.

Due to the growth conditions highly dislocated crystals were produced, which could be seen as a model system for dislocation clusters in directional solidified multicrystalline silicon ingots or for wafers grown by sheet growth techniques (e.g. RGS), which often exhibit high dislocation densities.

2 SAMPLE PREPARATION

In this section the growth of intentionally contaminated Si wafers and the preparation of lifetime and DLTS samples are presented.

All ingots doped with different concentrations of iron (Fe) and molybdenum (Mo) were grown at the Institute for crystal growth (IKZ) in the framework of the European integrated project Crystal Clear. In this work the iron contaminated material with a medium concentration of iron is investigated. The highest concentration was used for DLTS measurements to confirm, that the DLTS peaks in the as-grown state are related to the iron concentration and hence are iron-containing complexes (see section 5.1).

Using the pedestal growth method [1] with a monocrystalline seed crystal, 1.5 inch rods were grown and subsequently cut into 370 µm thick wafers. The Si feedstock was boron doped resulting in p-type wafers with a resistivity of 0.8 Ωcm, confirmed with Hall measurements performed at the University of Constance. Around $3 \cdot 10^{18}$ cm⁻³ iron was added to the melt, resulting

in a total iron concentration of $2 \cdot 10^{13}$ cm⁻³, confirmed with Neutron Activation Analysis (NAA) [2].

For the preparation of samples used for lifetime measurements the wafers were shiny etched resulting in a thickness of around 300 µm and were surface passivated by PECVD-SiN. The deposition temperature was around 350°C for approximately 40 minutes. Temperature dependent measurements were conducted in a cryostat capable of housing a 25x25 mm² sample. For this reason the 1.5 inch wafers were cut into a 25x25 mm² centre piece leaving four segments of the rim on which PL spectroscopy measurements in the as-grown state were conducted.

For DLTS measurements shiny etched samples were fully covered by 2 µm evaporated Al on the rear side to form an ohmic contact. On the front side Ti, Pd and Ag were evaporated establishing Schottky contacts. Using a shadow-mask, circular contacts having a diameter of 0.5 and 1 mm have been formed. The temperature during deposition remained below 100°C.

With these samples the as-grown state has been characterised and measurements and results are labelled as “as-grown” in what follows. During TLDS measurements (see section 3.2) the sample was measured several times at higher temperatures of around 260°C and subsequently slowly cooled down to room temperature with a rate of around 3°C/min. All together the sample was annealed for around 35 h at 260°C. To achieve a similar temperature profile for the “annealed” DLTS sample, the low temperature annealing was imitated. To prevent in-diffusion of metal impurities coming from the contacts of the DLTS sample the contacts were chemically removed and subsequently the samples were annealed at 260°C in 5 sequences 7 h long each. Again slow cooling ramps of around 10°C/min were used. Finally the contacts were evaporated again and DLTS measurements could be conducted on the “annealed” sample.

3 MEASUREMENT METHODS

The wafers were analysed with a series of characterisation methods. To give a deeper insight in the methods and their measurement conditions, a few of them are discussed here in more detail.

3.1 Deep Level Transient Spectroscopy (DLTS)

DLTS measurements were performed by means of transient Fourier spectroscopy in a DL-8000 Accent system. Principles of the system are described in [3]. In this method the capacitance transients are digitalized and the discrete Fourier coefficients are calculated from Fourier transformation of the transient. The coefficients are later used to calculate the amplitude and time constant of transients for a trap level.

3.2 Temperature Dependent Lifetime Spectroscopy

TDLS [4] is a method where a temperature dependent measurement is evaluated. In this case it is based on the microwave-detected photo conductance decay (MW-PCD) technique. This method is realised in our setup by embedding the sample in a nitrogen flooded cryostat, capable of cooling or heating the sample between -196°C and $+300^{\circ}\text{C}$. The sample is illuminated with a pulsed 908 nm laser and the excess carrier density is detected via changes in the microwave reflectance. Additionally the sample is irradiated by a bias light adjusting the background carrier concentration.

3.3 Photoluminescence (PL) spectroscopy

In our PL setup the sample is irradiated by a focused 532 nm laser. The irradiated sample emits luminescence light, which basically consists of the band-to-band and the defect luminescence. The luminescence light is guided through an optical system, spectrally expanded by an optical grating and detected by an InGaAs camera. This allows grabbing the whole luminescence spectrum within one exposure time. The sample is cooled to -196°C in order to increase the defect luminescence.

4 MEASUREMENT RESULTS

Different characterisation methods were applied on the iron contaminated sample in the as-grown state as well as after annealing. Results of each method are shown in the following.

4.1 DLTS results

DLTS measurements were performed on the as-grown sample and were compared to the sample after annealing. The result is shown in Fig. 1.

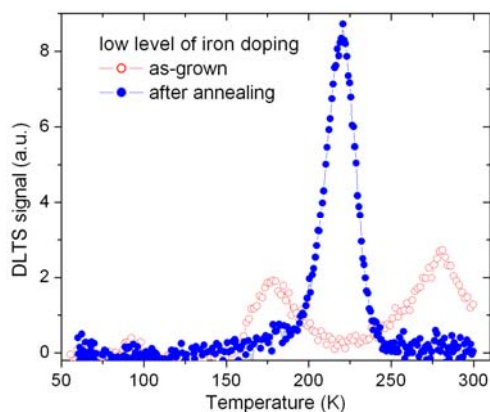


Figure 1: DLTS measurement on the iron doped sample (low level of iron doping) in as-grown state (red open points) and after low temperature annealing (blue points).

In the as-grown state two peaks are visible with energy levels of 0.33 and 0.52 eV above the valence band. Comparing the parameter of the first peak (180 K) to references [5-7], it could be assigned to an iron-related complex.

Both of these peaks vanish after annealing and a new peak arises. The energy level of this newly composed defect centre is $E_t = 0.44$ eV above the valence band with a capture cross section for holes of $\sigma_p = 1 \cdot 10^{-15} \text{ cm}^2$. The concentration of this defect centre is $N_t = 6 \cdot 10^{13} \text{ cm}^{-3}$. Due to the sample properties, these defect parameters are only approximations, however, comparing them to references [8-10], this peak could clearly be assigned to interstitial iron (Fe_i).

4.2 TDLS results

Temperature dependent lifetime measurements were performed to investigate the temperature dependence of minority carrier lifetime and to get information about the limiting defect centre for minority carriers. As shown in Fig. 2 (red open points) the lifetime was measured for temperatures between room temperature and 280°C . For the as-grown sample the lifetime is quite low and nearly temperature independent. On the as-grown sample, high temperature measurements ($100^{\circ}\text{C} - 270^{\circ}\text{C}$) were conducted several times, showing rising lifetimes for each measurement (not shown in Fig. 2). Finally the annealed sample was measured (Fig. 2, blue points).

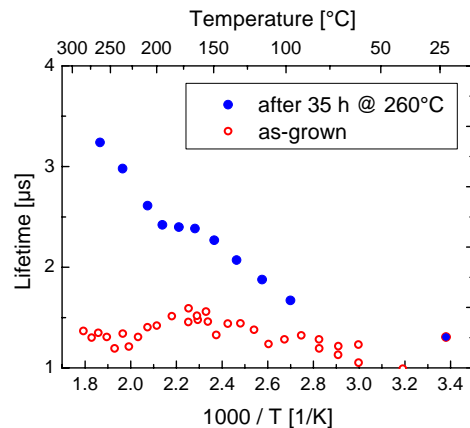


Figure 2: TDLS measurement on an iron doped sample in as-grown state and after a low temperature annealing.

After the annealing the slope of the curve has changed. The graph has a kink at around $150^{\circ}\text{C} - 200^{\circ}\text{C}$. The curve was re-measured after several months, resulting in an almost equal curve (not shown in Fig. 2). A repeated low temperature anneal of around 6 h at 300°C further raised the lifetime, but didn't change the shape of the curve.

4.3 PL spectroscopy results

Photoluminescence spectroscopy measurements were conducted to evaluate the spectral emission of carriers during recombination. This was performed on several points of the "annealed" centre piece, as well on several points of some segments of the rim which remained in the as-grown state and were not subject to annealing.

The PL spectra for different points on each sample are almost identical, one representative curve is shown in

Fig. 3 for each state, red representing the as-grown state, whereas the blue curve corresponds to the sample after annealing.

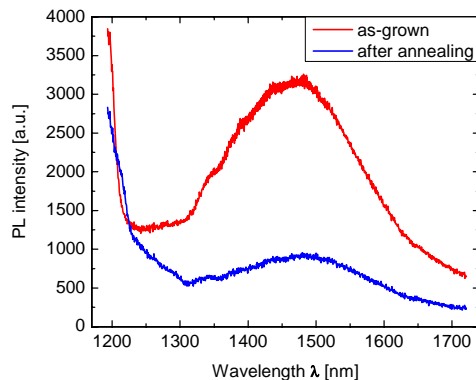


Figure 3: PL spectroscopy on the iron contaminated sample before and after the low temperature annealing.

At shorter wavelength ($\lambda < 1200$ nm) the signal for both samples is dominated by band to band luminescence, which is mainly determined by the minority carrier density and should not be further considered here. The luminescence behaviour changes for longer wavelengths where the signal is generated by recombination via dislocations, leading to typical dislocation lines (D1-D4). Due to the insufficient resolution of our measurement setup no separated dislocation-related peaks could be resolved but a superposition of several defect lines could be seen. As the maximum is around 1450-1500 nm the D2 line has a major contribution to the signal, but is superimposed by further defect lines.

The striking feature in Fig. 3 is the difference between annealed and non-annealed sample. The latter, which stayed in the as-grown state, has a much higher dislocation-related signal than the annealed sample.

5 DISCUSSION OF THE EFFECT OF LOW TEMPERATURE ANNEALING

An iron doped sample was prepared using the pedestal growth method. Wafers were processed to contacted DLTS or SiN surface passivated lifetime samples and were characterised with DLTS, TDLS and PL spectroscopy in two different states, i.e. as-grown and after a low temperature annealing for prolonged time. All characterisation methods show a clear change of sample properties after annealing. A more detailed discussion on each characterisation result is given in the following.

5.1 Transformation of iron-related complexes to interstitial iron observed with DLTS

The DLTS signal (Fig. 1) showed two peaks in the as-grown state. The first peak at around 180 K could be assigned to an iron oxygen related complex. Wünnel and Wagner [7] reported a defect centre with $E_v+0.33$ eV after Fe in-diffusion in Cz Si followed by a slow cooling. It was assigned to a complex of iron with oxygen. Pearton and Tavendale [6] found a very similar Fe-O level as Wünnel with an energy level of $E_v+0.32$ eV. The same complex was also observed by Castaldini et al. [5] in their slow-cooled samples having an equal energy of

$E_v+0.33$ eV, but it was assigned to a complex involving Fe and several oxygen atoms $\{FeO_n\}$. Estreicher [11] calculated binding energies for a $\{Fe_3O_i\}$ complex formed of Fe_i and an oxygen vacancy pair during 800-1000 K treatment to 3.9 eV. However, such high binding energies would prevent bonds from breaking up during annealing at moderate temperatures, for this reason assignment of the observed complex to the $\{Fe_3O_i\}$ [11] is less probable. Further calculations of Estreicher showed no interaction between Fe_i and interstitial oxygen or an oxygen dimer respectively, an indication against a iron complex with several oxygen atoms.

For the second peak of the as-grown sample situated at around 280 K no matching reference was found. An energy level of 0.52 eV and a capture cross section for holes of $6 \cdot 10^{-14} \text{ cm}^2$ have been found for this centre. Hence, the defect is unlikely to be Fe_i .

It should be noted that the detected DLTS peaks are not much different from those reported for the dislocations and oxide precipitates in silicon [12]. However, absence of the DLTS signals after the annealing procedures makes such an assignment also less probable. We conclude that the origin of the peaks is not clear at the moment, however their relation to iron is highly probable as will be further supported below.

Estreicher calculated a lot of possible iron related centres in Si [11], however iron-related extended defects like precipitates, dislocations or grain boundaries is a topic which is still unclear.

To further evaluate whether the detected peaks are iron related, a sample with a strong iron doping is compared to the previous one. The sample has been grown with the same technique but adding more iron in the silicon melt. DLTS measurements on both samples are shown in Fig. 4.

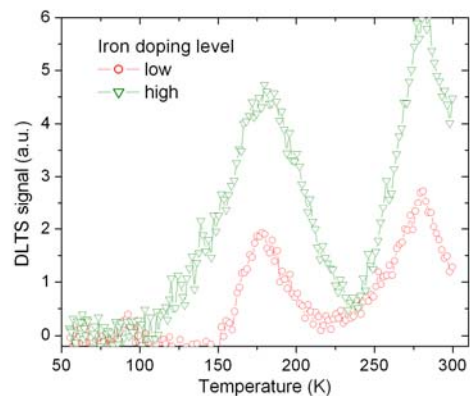


Figure 4: DLTS measurement on two iron doped samples with different iron concentrations. Both samples are in the as-grown state. The DLTS signal of the lowly doped sample is shown in red (same curve as in Fig. 1), the green points correspond to measurement points of the highly iron doped sample.

Both samples show the two peaks discussed above. The only difference between both samples is the concentration of the corresponding defects, affecting the intensity of the peak. The higher iron doping ends up with an enhanced defect concentration.

To conclude the DLTS measurements, it could be said that iron related defects decompose during the low temperature anneal and form interstitial iron.

5.2 Formation of interstitial iron observed with TDLS

This conclusion could be clarified with TLDS measurements. The lifetime at higher temperatures increases during the annealing and the temperature dependence alters. From the kink in the curve, it could be seen that the temperature dependence of the curve changes, leading to the conclusion that the type of defect has changed. From the fact that this changing occurs at around 180°C, which is exactly the temperature where FeB pairs split into substitutional boron and interstitial iron, this kink indicates that iron boron pairs split and the more recombination active interstitial iron is responsible for the TDLS curve at temperatures higher than 200°C.

Further measurements revealed that this state is stable at room temperature, leading to the conclusion that a non-equilibrium defect configuration present in the as-grown wafer could be transformed into a stable state, which is thought to be FeB or Fe_i, respectively, depending on the temperature.

5.3 Reduction of dislocation luminescence explained by the Kveder model

The striking feature in Fig. 3 is the difference between annealed and non-annealed sample. The latter, which stayed in the as-grown state, has a much higher signal generated by radiative emission via dislocations. An enhanced lifetime for the annealed sample (observed with TDLS) would generally result in a higher PL intensity, what could also be observed in the band-to-band luminescence light at $\lambda < 1200$ nm. Nevertheless the dislocation luminescence is much smaller for the annealed sample.

The influence of impurity decoration on the dislocations luminescence and on the recombination behavior of dislocations has been investigated by e.g. Kveder et al. [13] and Kittler et al. [14]. Kveder proposed a model for the recombination processes at dislocations. This model successfully describes the temperature- and intensity-dependent contrast observed in electron-beam induced current (EBIC) measurements in the vicinity of clean and decorated dislocations.

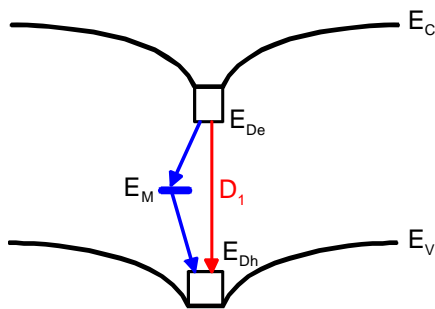


Figure 5: Band structure in a vicinity of a dislocation with two possible recombination mechanisms (Kveder model [13]). A positively charged dislocation creates a band bending of the valence E_V and the conduction band E_C , whereas the dislocation bands E_{De} and E_{Dh} originate from the strain field of a dislocation. Transitions are possible on the direct way (D_1 line, shown in red), as well as over a deep level E_M (blue).

In Fig. 5 a simple schema is shown, explaining the possible carrier transitions near to a dislocation,

assuming p-type Si with a positively charged dislocation. The band bending is caused by the electrical charge of the dislocation. The defect bands E_{De} and E_{Dh} originate from the strain field of the dislocation [13]. Additionally, deep levels generated by transition metals situated at the dislocation core or attached in its strain field could exist generating a competing non-radiative recombination path (Fig. 5, blue). For non-decorated dislocations the main recombination process will be the radiative recombination between the dislocation bands, resulting in the typical dislocation lines. The most common defect luminescence lines are D1-D4 with wavelength from 1537 nm to 1253 nm [15].

Considering the results seen in DLTS and TDLS measurements, that an iron-related defect centre could be transformed to interstitially dissolved iron, following process is proposed explaining the decreasing photoluminescence signal after annealing. During the low-temperature annealing iron-related complexes dissolve and a part of the emerged interstitial iron atoms diffuse to the dislocations, accumulate there and form iron decorated dislocations.

The case of direct recombination between dislocation bands could be found in the as-grown sample, where a high luminescence signal was found around 1500 nm. This means that a part of the dislocations are not decorated. This behaviour changes during annealing where iron-containing complexes are dissolved and the emerged interstitial iron atoms could decorate dislocations, resulting in a deep energy level in the band gap, creating the competing non-radiative transition path over Shockley-Read-Hall recombination (SRH). Now, the most active recombination process is the non-radiative transition via deep levels. Hence, the radiative recombination process, generating PL light around $\lambda = 1300-1600$ nm, is suppressed, yielding a lowered luminescence signal at around 1500 nm what could be observed in Fig. 3. Higgs observed a similar effect on intentionally copper contaminated dislocations, showing that with higher initial copper concentrations (over a certain threshold) the PL intensity decreases strongly [16]. We could therefore suppose that a lower contamination of dislocations in the as-grown state resulted in a higher PL signal.

In supposition of decomposing iron-containing defects the DLTS peaks could be explained, as well as the shape of the TDLS measurements and the PL spectroscopy findings. However, the type of defect in the as-grown state related to the DLTS peak at around 280 K remains unclear as well as its high recombination activity resulting in a very low lifetime in the as-grown state.

The results of our measurements all indicate that an iron containing defect dissolves during the low temperature anneal. However, dissolution of precipitates would only be possible at high temperatures once you have undersaturated silicon. For this reason a precipitate will always grow rather than dissolve at temperatures around 300°C. This would imply that not iron precipitates dissolve during the low temperature annealing, but some other form of an iron-containing complex (e.g. iron-oxygen or iron-silicide complexes) decomposes and releases interstitial iron atoms.

The reason for the very low lifetime of as-grown wafers keeps unknown. We can suppose that iron-related complexes formed during the crystallisation affected the growth conditions, generating a highly dislocated crystal

with iron-related complexes, which in combination are responsible for the low lifetime, as well as for the fact that the sample is in no equilibrium configuration after the crystal growth.

6 CONCLUSION

Intentionally iron contaminated samples were investigated in the as-grown state and after a prolonged low temperature anneal with different characterisation techniques, i.e. DLTS, TLDS and PL. A defect transformation was found, changing the type of defect from iron-related complexes to interstitial iron. The observed PL spectra could be explained by applying Kveder's model, i.e. that additional deep levels, introduced by the decomposition of iron related complexes, could reduce the radiative transition between dislocation bands.

ACKNOWLEDGEMENTS

This work has been carried out as part of the CrystalClear Integrated Project, with financial support from the European Commission under contract number SES6-CT_2003-502583.

The authors would like to thank M. Kasemann and J. Schön for many fruitful discussions and H. Lautenschlager for the processing of DLTS contacts

REFERENCES

- [1] T.F. Cizek, *Journal of Crystal Growth* **66**, 655 (1984).
- [2] G. Coletti, et al., *Proceedings of the 22nd European Photovoltaic Solar Energy Conference*, Milan, Italy, 989 (2007).
- [3] S. Weiss, et al., *Solid-State Electronics* **31**, 1733 (1988).
- [4] S. Rein, *Lifetime spectroscopy: a method of defect characterization in silicon for photovoltaic applications*, (Springer, Berlin, 2005).
- [5] A. Castaldini, et al., *Applied Physics Letters* **86**, 162109 (2005).
- [6] S.J. Pearton, et al., *Journal of Physics C: Solid State Physics* **17**, 6701 (1984).
- [7] K. Wünnel, et al., *Solid State Communications* **40**, 797 (1981).
- [8] J.L. Benton, et al., *Journal of The Electrochemical Society* **129**, 2098 (1982).
- [9] K. Graff, *Metal Impurities in Silicon-Device Fabrication*, Vol. 24, 2nd ed., (Springer, Berlin, 1999).
- [10] K. Nakashima, et al., *Jpn. J. Appl. Phys.* **25**, 234237 (1986).
- [11] S.K. Estreicher, et al., *Physical Review B (Condensed Matter and Materials Physics)* **77**, 125214 (2008).
- [12] T. Mchedlidze, et al., *Japanese Journal of Applied Physics, Part 1 (Regular Papers & Short Notes)* **38**, 3426 (1999).
- [13] V. Kveder, et al., *Physical Review B* **63**, 115208 (2001).
- [14] M. Kittler, et al., *Microelectronic Engineering* **66**, 281 (2003).
- [15] S. Pizzini, et al., *Physica Status Solidi B* **222**, 141 (2000).
- [16] V. Higgs, et al., *Applied Physics Letters* **60**, 1369 (1992).